Human Molecular Genetics, 2021, Vol. 30, No. 9 823–835

doi: 10.1093/hmg/ddab032
Advance Access Publication Date: 30 January 2021
Association Studies Article

ASSOCIATION STUDIES ARTICLE

Post-GWAS functional studies reveal an RA-associated *CD40*-induced NF-kB signal transduction and transcriptional regulation network targeted by class II HDAC inhibitors

Meijuan Zou[1,2], Danli Jiang[1], Ting Wu[1,3], Xiaoyu Zhang[1], Yihan Zhao[1], Di Wu[4], Wei Sun[5], Jing Cui[6], Larry Moreland[7,†] and Gang Li[1,8,*,†]

[1]Aging Institute, University of Pittsburgh, Pittsburgh, PA 15219, USA, [2]Department of Pharmacology, Nanjing Medical University, Nanjing 211166, China, [3]Department of Medicine, Xiangya School of Medicine, Central South University, Changsha 410083, China, [4]Department of Periodontology, University of North Carolina at Chapel Hill, Chapel Hill, NC 27599, USA, [5]Department of Medicine, Center for Pulmonary Vascular Biology and Medicine, Pittsburgh Heart, Lung, Blood, and Vascular Medicine Institute, University of Pittsburgh Medical Center, Pittsburgh, PA 15261, USA, [6]Department of Medicine, Division of Rheumatology, Immunology and Allergy, Brigham and Women's Hospital, Boston, MA 02115, USA, [7]Department of Medicine, Division of Rheumatology, University of Pittsburgh Medical Center, Pittsburgh, PA 15261, USA and [8]Department of Medicine, Division of Cardiology, University of Pittsburgh Medical Center, Pittsburgh, PA 15261, USA

*To whom correspondence should be addressed at: Department of Medicine, Division of Cardiology, University of Pittsburgh Medical Center, Bridgeside Point 1, Room 561, 100 Technology Drive, Pittsburgh, PA 15219, USA. Tel: +1 8574724787; Fax: +1 4123839055; Email: lig@pitt.edu

Abstract

Currently, it remains difficult to identify which single nucleotide polymorphisms (SNPs) identified by genome-wide association studies (GWAS) are functional and how various functional SNPs (fSNPs) interact and contribute to disease susceptibility. GWAS have identified a *CD40* locus that is associated with rheumatoid arthritis (RA). We previously used two techniques developed in our laboratory, single nucleotide polymorphism-next-generation sequencing (SNP-seq) and flanking restriction enhanced DNA pulldown-mass spectrometry (FREP-MS), to determine that the RA risk gene *RBPJ* regulates *CD40* expression via a fSNP at the RA-associated *CD40* locus. In the present work, by applying the same approach, we report the identification of six proteins that regulate *RBPJ* expression via binding to two fSNPs on the RA-associated *RBPJ* locus. Using these findings, together with the published data, we constructed an RA-associated signal transduction and transcriptional regulation network (STTRN) that functionally connects multiple RA-associated risk genes via transcriptional regulation networks (TRNs) linked by *CD40*-induced nuclear factor kappa B (NF-kB) signaling. Remarkably, this STTRN provides insight into the potential mechanism of action for the histone deacetylase inhibitor givinostat, an approved therapy for systemic juvenile idiopathic arthritis. Thus, the generation of disease-associated STTRNs based on post-GWAS

[†]Gang Li, http://orcid.org/0000-0003-1725-6611
[†]Present address: Department of Medicine, Division of Rheumatology, University of Colorado, Aurora, CO 8004, USA.
Received: November 23, 2020. **Revised:** January 8, 2021. **Accepted:** January 20, 2021

functional studies is demonstrated as a novel and effective approach to apply GWAS for mechanistic studies and target identification.

Introduction

Rheumatoid arthritis (RA) is an autoimmune disease that affects 0.5–1% of the population. It is a long-term, progressive and disabling disease, resulting in destructive inflammation, swelling and pain in the joints and other tissues and organs. The pathogenesis of RA remains incompletely understood and there is no effective cure (1).

As a complex disease, RA susceptibility is believed to be associated with multiple genes in combination with environmental factors. While genome-wide association studies (GWAS) have identified and validated more than 100 genetic loci that are associated with RA (2), post-GWAS functional studies have proven to be extremely difficult owing to the fact that the single nucleotide polymorphisms (SNPs) used by GWAS to pinpoint these genetic loci are simply a proxy for large stretches of DNA (haplotypes) that contain many other SNPs in linkage disequilibrium (LD), most of which reside in non-coding DNA (3). Similarly, even though a handful of environmental factors have been documented to have relatively consistent associations with RA (4), delineating how each of the environmental factors contributes to RA pathogenesis is equally difficult without understanding the biological mechanisms underlying the contribution of RA risk genes to the disease.

CD40 is a member of the TNF-receptor superfamily, which is mainly expressed on antigen presenting cells such as B cells, dendritic cells and macrophages. Upon ligation of *CD40* with its ligand CD40L, a multitude of signaling pathways are activated, including the nuclear factor kappa B (NF-kB) pathway, which mediate a broad range of immune and inflammatory responses (5). Recent large GWAS have validated seven RA associated loci that are involved in *CD40*-induced NF-kB signaling; they are: *CD40*, *RBPJ*, *TNFAIP3*, *TRAF1*, *TRAF6*, *NFKBIE* and *REL* (6). Previously, we demonstrated that the disease-associated *CD40* locus is a gain-of-function allele with more *CD40* expression on the risk allele, which, upon CD40L activation, results in a high level of activation of NF-kB p65 (RelA) by phosphorylation (7). In order to understand the mechanisms underlying the contribution of RA-associated functional SNPs (fSNPs), recently, we developed two novel techniques: single nucleotide polymorphism-next generation sequencing (SNP-seq) and flanking restriction enhanced DNA pulldown-mass spectrometry (FREP-MS) (8). By coupling SNP-seq with FREP-MS, we identified *RBPJ* as one of the four transcriptional regulators modulating *CD40* expression via three fSNPs on the *CD40* locus (8). Interestingly, *RBPJ* itself is also an RA risk gene (6,9).

The *CD40*–CD40L axis is involved in many diseases, including autoimmune diseases and cardiovascular diseases (10,11). Blocking the interaction between *CD40* and CD40L has proved effective in preventing these diseases or in ameliorating their symptoms. This suggests that *CD40* is a potential target for drug development (11). However, there is currently no approved drug that inhibits *CD40*–CD40L signaling since early efforts induced significant side effects (7). Human genetics suggests that inhibiting *CD40*-mediated intracellular signaling could be effective in humans (7). However, human genetics also suggests that *CD40* is not the only risk gene linked to RA. Indeed, it may very well be a combination of multiple risk genes, which seemingly have no connection, that form a presently uncharacterized genetic network that ultimately determines a person's overall immune response and susceptibility to RA.

Systems biology is a study of biological systems that integrate key elements such as DNA, RNA, proteins and cells as a whole network (12). Based on the data generated by GWAS, we hypothesize that there are disease-associated risk gene transcriptional regulation networks (TRNs) linked by signal transduction pathways in a cell type-specific fashion. We refer to this network as signal transduction and transcriptional regulation network (STTRN). Obviously, the pathogenesis and/or susceptibility of a complex disease is not because of the signal transduction pathway itself, but the perturbation of a set of risk gene expression, presumably by transcriptional regulation via the risk alleles of many causative fSNPs. In such a network, change in one single gene expression in response to an environmental factor could alter the expression of all the risk genes in this network. If all the alleles in this risk network predispose toward disease risk, a destructive signal, possibly initiated by an environmental factor such as smoking, would be amplified. However, at the current stage, our knowledge on gene transcriptional regulation, especially on disease-associated risk gene transcriptional regulation, is extremely limited; therefore, it is difficult to construct a disease-associated STTRN. GWAS, as a tool to study complex disease, provides a window of opportunity to collect the disease-associated functional information required to build such a STTRN.

In this study, using SNP-seq and FREP-MS, together with allele-imbalanced DNA pulldown-western blot (AIDP-Wb), a novel DNA pulldown assay recently developed in our laboratory to specifically detect the allele-imbalanced binding of a known protein to a fSNP (13), we screened a library containing 156 SNPs collected from the seven aforementioned RA loci in LD with $r^2 > 0.8$ on the *CD40*-induced NF-kB signal pathway. We validated two fSNPs on the *RBPJ* locus together with six regulatory proteins that modulate the *RBPJ* expression. Based on these findings, as well as previous publications, we constructed and verified an RA-associated STTRN involving the *CD40*-induced NF-kB signaling, using both RNAi gene knockdown and histone deacetylase (HDAC) inhibition in human B cells and fibroblast-like synoviocytes (FLS).

Results

Identification and validation of two fSNPs on the RA-associated *RBPJ* locus

Previously, we introduced SNP-seq to identify four RA-associated fSNPs on the RA-associated *CD40* locus (8). In the present work, we applied SNP-seq to screen a DNA library containing 156 SNPs in LD with $r^2 > 0.8$ collected from the seven RA risk loci involved in the *CD40*-induced NF-kB pathway, including *CD40*, *RBPJ*, *TRAF1*, *TRAF6*, *NFKBIE*, *REL* and *TNFAIP3* (6), as outlined in Supplementary Material, Figure S1A. The quality of the screen is evidenced by high reproducibility between two technical repeats with a correlation coefficient demonstrating an $r^2 = 0.8893$ (Supplementary Material, Fig. S1B). As a result, we identified 69 candidate fSNPs with a *P*-value < 0.05 and a Slope > 0.05 and < -0.05 (Supplementary Material, Table S1). Within these 69 candidate fSNPs, we recovered the four fSNPs (rs4810485,

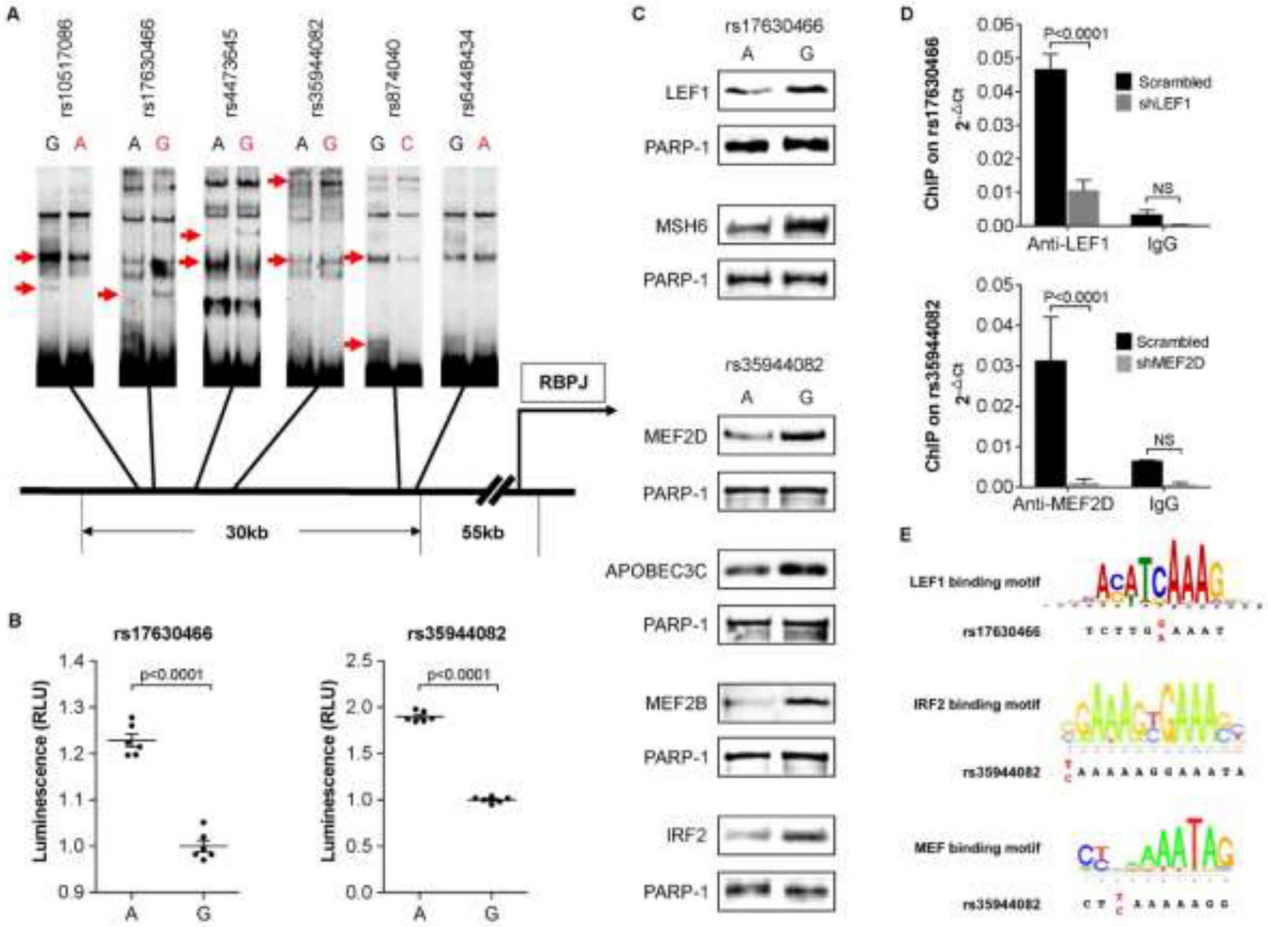

Figure 1. Identification and characterization of rs17630446 and rs35944082 in the RA-associated *RBPJ* locus. (**A**) EMSA showing allele-imbalanced gel shifting on six candidate fSNPs on the *RBPJ* locus in LD with rs874040. Red nucleotides indicate the risk alleles on each SNP. Red arrows indicate the allele-imbalanced shifting bands. The data represent three biological replicates ($n = 3$). (**B**) Luciferase reporter assays demonstrating fSNPs rs17630466 and rs35944082. The data represent a combination of six biological replicates ($n = 6$). RLU: relative luminescent unit. (**C**) AIDP showing allele-imbalanced binding of LEF1 and MSH6 specifically bound to rs17630466 and IRF2, APOBEC3C, MEF2B and MEF2D to rs35944082. PARP-1 was used as internal loading control. The data represent three biological replicates ($n = 3$). (**D**) ChIP assays demonstrate the specific binding of LEF1 to rs17630466 and MEF2D to rs35944082. The data represent a combination of three biological replicates ($n = 3$). Ct: cycle threshold; IgG: immunoglobulin G (**E**) Motif analyses reveal the sequence similarity between the LEF1 binding sequence and the sequence from rs17630466 and between the IRF2 and MEF binding sequence and the sequence from rs35944082. Red nucleotides indicate SNPs. sh, shRNA; NS, non-significant.

rs1883832, rs6032664 and rs6056926) on the RA-associated *CD40* locus which we previously identified and confirmed (8). Among the remaining 65 candidate fSNPs, we identified six SNPs (rs10517086, rs17630466, rs4473645, rs35944082, rs874040 and rs6448434) among 13 SNPs on an RA-associated *RBPJ* locus in LD with rs874040 ($r^2 > 0.8$). Among these six candidate fSNPs, five SNPs except for rs6448434 were demonstrated as fSNPs by electrophoretic mobility shift assay (EMSA) as each identified fSNP showed allele-imbalanced gel shifting (Fig. 1A). To further validate these five fSNPs, as a proof of evidence, we performed a luciferase reporter assay on two of these five fSNPs; they were rs17630466 and rs35944082. As noted, an allele-imbalanced luciferase activity between the two alleles of each of these two fSNP was evident (Fig. 1B). In both cases, the risk allele G has lower luciferase activity than the non-risk allele A, suggesting that both SNPs are likely bind to suppressive regulators.

We also performed *in silico* analysis on the 13 SNPs in LD with rs874040 ($r^2 > 0.8$) using HaploReg 4.1, a web-based tool for epigenetic and functional annotation of genetic variants (14). Using Haploreg, we scored each of the 13 SNPs on a scale of 0–5 to reflect the number of positive annotations for promoter and enhancer histone methylation generated by ChIP-seq, DNase hypersensitivity by DNase-seq and predicted protein binding and alteration in binding motifs (Supplementary Material, Table S2). Among the six candidate SNPs we identified, both rs35944082 and rs874040 scored 5 (together with one non-fSNP), rs4473645 scored 3, rs17630466 and rs6448434 scored 2 and rs10517086 scored 1, suggesting a moderate enrichment of fSNPs in this analysis.

Identification of regulatory proteins that specifically bind to fSNPs rs17630466 and rs35944082 modulating *RBPJ* expression

All 156 SNPs in the library we screened are in the non-coding region of human DNA; therefore, they do not change protein coding sequences. Instead, they presumably exert their functions by binding to unknown regulatory proteins to control risk gene expression (15–20). To understand how the two fSNPs,

rs17630466 and rs35944082, identified on the *RBPJ* locus modulate *RBPJ* expression, we performed FREP-MS on these two fSNPs using the G allele (risk allele) from both rs17630466 and rs35944082. We chose the G alleles since they show more protein binding in the allele-imbalanced gel shifting for both fSNPs (Fig. 1A). To increase specificity, we performed FREP-MS with these two fSNPs in parallel so that we can use these two fSNPs as specificity controls for each other (8). To further increase the fidelity, we performed this FREP-MS analysis with each SNP in duplicate. By doing so, based on the specific peptide spectrum counts shown in Supplementary Material, Table S3, we identified two proteins, LEF1 and MSH6, that specifically bind to rs17630466 and four proteins, IRF2, APOBEC3C, MEF2B and MEF2D, that bind to rs35944082. While all these proteins were reported as transcriptional regulators, MSH6 is a DNA mismatch repair protein that has never been documented as a transcription factor (21). Moreover, among these proteins, only MEF2 could be identified as a protein specifically binding to fSNP rs35944082 using *in silico* analysis (HaploReg 4.1; Supplementary Material, Table S2).

To demonstrate that LEF1 and MSH6 bind to rs17630466 and IRF2, APOBEC3C, MEF2B and MEF2D bind to rs35944082, respectively, we applied AIDP-Wb (13). Using this method, we observed an allele-imbalanced binding of LEF1 and MSH6 to rs17630466 and IRF2, APOBEC3C, MEF2B and MEF2D to rs35944082, respectively (Fig. 1C). In both cases, the risk allele G binds more of these factors than the non-risk allele A. The noted allele-imbalanced binding of these regulatory proteins to rs17630466 and rs35944082 showed in this assay further validates that rs17630466 and rs35944082 are indeed *bona fide* fSNPs. To further validate the specific binding of these proteins to the two fSNPs, as a proof of evidence, we performed chromatin immunoprecipitation (ChIP) assay on rs17630466 using an anti-LEF1 antibody and on rs35944082 using an anti-MEF2D antibody. A significant decrease in the binding of LEF1 to a DNA fragment containing rs17630466 and MEF2D to a DNA fragment containing rs35944082 was observed when we compared BL2 cells, a human B cell line, with either *LEF1* or *MEF2D* shRNA knockdown to a scrambled shRNA control (Fig. 1D). In addition, the binding of LEF1 to rs17630466, as well as IRF2 and MEF2B/D to rs35944082, was further supported by the sequence similarity between these protein binding motifs (22,23) (ISMARA) and the sequences from the two fSNPs (Fig. 1E). Together, these data support that there is the specific binding of LEF1 and MSH6 to rs17630466 and the specific binding of IRF2, APOBEC3C, MEF2B and MEF2D to rs35944082.

To demonstrate that LEF1 and MSH6 as well as IRF2, APOBEC3C, MEF2B and MEF2D are the transcriptional regulators modulating *RBPJ* expression, we knocked down each of these proteins in BL2 cells using lentiviral shRNA. As a result, we observed that knockdown of each of these six proteins increases the expression of *RBPJ* at both the protein level, detected by western blots (Fig. 2A), and the mRNA level, detected by qPCR (Fig. 2B). These data, consistent with the data from the allele-imbalanced luciferase reporter assay presented in Figure 1B, suggest that all these six proteins function as *RBPJ* suppressors, with the risk allele G binding more of these proteins and having lower luciferase activity than the non-risk allele A. Previously, we showed that *RBPJ* is a transcription suppressor of *CD40* via binding to the fSNP rs4810485 on the RA-associated *CD40* locus (8). Consistent with this data, we also observed a decreased *CD40* expression in all these six knockdown BL2 cell lines (Fig. 2), which further demonstrates the suppressive function of these six proteins in regulating *RBPJ* expression.

Class II HDAC inhibitors trigger a TRN from *HDAC7* to *MEF2D*, *RBPJ* and *CD40* in human B cells

MEF2D was recently reported to be associated with a systemic lupus erythematosus (SLE) sub-phenotype in Swedish cohorts (24). Like RA, SLE is also an autoimmune disease, resulting from the immune system mistakenly attacking its own body; therefore, these conditions share several clinical and pathological features as well as underlying biological mechanisms (25). Also, previously, it was reported that the expression of *MEF2D* is regulated by HDACs since treating human myocytes with the class II HDAC inhibitor MC1568 decreases *MEF2D* expression (26). MC1568, a derivative of (aryloxopropenyl)pyrrolyl hydroxyamide, is a novel, potent and specific inhibitor of class II HDACs. To determine if MC1568 regulates *MEF2D* expression in human B cells, we treated BL2 cells with different concentrations of MC1568. Significant downregulation of *MEF2D* was observed at both the mRNA and protein levels (Fig. 3A and C). To confirm this data, we used another HDAC inhibitor, ITF2357, also known as givinostat, to treat the BL2 cells. ITF2357 is a potent inhibitor of both class I and class II HDACs as well as an approved drug in the European Union for the treatment of systemic juvenile idiopathic arthritis (SJIA) (27). Our results showed that the treatment with ITF2357 also decreased the expression of *MEF2D* in BL2 cells (Fig. 3B and C). These data demonstrate that *MEF2D*, as a SLE risk gene, is regulated by class II HDACs. Again, consistent with our findings in the *MEF2D* shRNA knockdown BL2 cells (Fig. 2), we also observed a significant upregulation of *RBPJ* and downregulation of *CD40* expression in either MC1568- or ITF2357-treated BL2 cells (Fig. 3A–C).

Both *HDAC4* and *HDAC7* belong to class II HDACs and can be inactivated by MC1568 (26,28). To identify which one of these two HDACs is involved in the regulation of *MEF2D*, we performed siRNA knockdown on *HDAC7* and *HDAC4* in human FLS. Downregulation of each of these genes resulted in decreased *MEF2D* expression, increased *RBPJ* expression and subsequent upregulation of *CD40* expression (Fig. 3D and E), suggesting that both *HDAC7* and *HDAC4* can regulate the *MEF2D* expression, possibly in the same transcriptional complex. Coincidently, *HDAC7* is also an RA risk gene (29).

Together, our findings reveal an RA-associated TRN in human cells linking *HDAC4*/*HDAC7* to *MEF2D*, *RBPJ* and *CD40*. Moreover, this network is targeted by class II HDAC inhibitors.

An RA-associated STTRN involving *CD40*-induced NF-kB signaling in human B cells

Previously, we demonstrated that, with increased cell surface *CD40* expression (as is the case for carriers of the RA risk allele), there is an increased activation of the classical NF-kB pathway as measured by the phosphorylation of NF-kB p65 in human B cells (7). To determine if the downregulation of *CD40* induced by *MEF2D* inactivation affects *NF-kB p65* activation, we first treated both the scrambled shRNA control and the *MEF2D* shRNA knockdown BL2 cells with MEGACD40L, a trimeric *CD40* ligand, at 64 ng/ml for 15 min as we described previously (7). Activation of NF-kB p65 was evaluated with an anti-phosphorylated p65 antibody. Consistent with our previous results, we observed a reduction of phosphorylated NF-kB p65 in the *MEF2D* knockdown BL2 cells (Fig. 4A). We also checked the activation of p65 by MEGACD40L in the BL2 cells treated with either MC1568 or ITF2357. In both cases, we also observed reduced phospo-NF-kB p65 in treated cells (Fig. 4B and C).

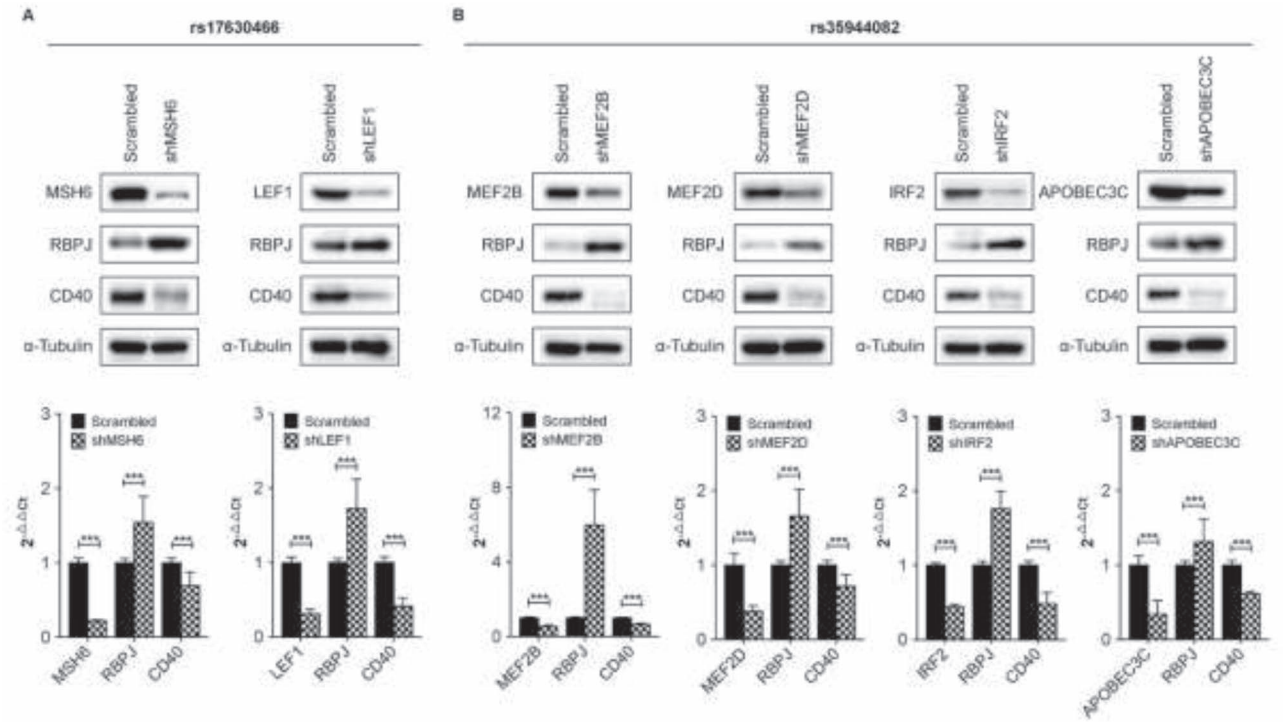

Figure 2. Western blots and qPCR assays demonstrate MSH6 and LEF1 as well as MEF2B, MEF2D, APOBEC3C and IRF2 as transcription suppressors of *RBPJ* in human BL2 cells. (**A**) Western blots and qPCR assays showing that knockdown of *MSH6* and *LEF1* with shRNA results in upregulation of *RBPJ* and downregulation of *CD40* in BL2 cells. (**B**) Western blots and qPCR assays showing that knockdown of *MEF2B, MEF2D, APOBEC3C* and *IRF2* with shRNA leads to upregulation of *RBPJ* and downregulation of *CD40* in BL2 cells. ***P-value < 0.001. The western blot data represent three biological replicates ($n = 3$). The qPCR data represent a combination of three biological replicates ($n = 3$). sh, shRNA Ct: cycle threshold.

NF-kB has long been known to play an important role in autoimmune diseases such as RA (30,31). *CD40*-induced NF-kB signaling in disease pathogenesis is highlighted by GWAS analysis in RA (2,32). Besides its role in the regulation of various pro-inflammatory genes, NF-kB also plays a critical role in regulating the expression of many other genes involved in cell survival, activation and differentiation of innate immune cells and inflammatory T cells (33). Based on TRRUST V2, a manually curated database of human and mouse transcriptional regulatory networks (34), we identified 17 NF-kB *p65* targeted genes that are associated with high risk RA (GWAS catalog, 2109). Among these, eight were reported to be regulated by *CD40* in human B cells: *CD83* (35), *CDK4*/*CDK6* (36), *c-FLIP* (37), *ICAM1* (38), *TNFAIP3* (39), *IRF4* (40) and *TRAF1* (41). We therefore performed qPCR on these eight RA risk genes, together with *IL6* and *IL1β*, the two key proinflammatory cytokines, in the *MEF2D* knockdown BL2 cells treated with MEGACD40L. As a result, we observed a significant downregulation in the expression of all these eight RA risk genes plus *IL6* and *IL1β* in the *MEF2D* knockdown BL2 cells compared with the scrambled controls (Fig. 4D). We also checked the expression of these eight RA risk genes plus *IL6* and *IL1β* in BL2 cells activated by MEGACD40L after either ITF2357 or MC1568 treatment. While we observed a similar downregulation of all these eight genes plus *IL6* and *IL1β* in the ITF2357-treated cells, a different expression pattern of these genes was identified in the MC1568-treated cells (Fig. 4E). The expression of *CDK4* and *CDK6* was not significantly changed, and the expression of *ICAM1*, *IL6* and *IL1β*, instead of being downregulated in the ITF2357-treated cells, was significantly upregulated in the MC1568-treated cells. Of note, only ITF2357 is approved for clinical use.

Together, these data demonstrate that there is an RA-associated *CD40*-induced STTRN. In this STTRN, an RA risk gene TRN from *HDAC7* to *MEF2D*, *RBPJ* and *CD40* is linked via the *CD40*-induced NF-kB signal transduction to another RA risk gene TRN from NF-kB *p65* to the eight RA risk genes, including *IL6* and *IL1β*.

An RA-associated CD40-induced NF-kB STTRN in primary human FLS

FLS are the main stromal cells of the joint synovium; therefore, they play a critical role in the etiology (e.g. cartilage destruction) of RA (42). To determine whether the RA-associated *CD40*-induced NF-kB STTRN exists in FLS, primary human FLS isolated from a patient with osteroarthritis (OA) were used owing to the unavailability of normal FLS. To make use of this FLS, we generated all our results by comparing the treated FLS with the same untreated FLS control. Primary human FLS were treated with 1 μm ITF2357 for 24 h and then activated by 64 ng/ml MEGACD40L for 15 min. Proteins were isolated from both treated samples and untreated controls for western blot analysis to assess the expression of *MEF2D*, *RBPJ*, *CD40* and phosphorylated NF-kB p65. Consistent with our results found in the ITF2357-treated human BL2 cells, we observed a similar downregulated *MEF2D*, increased *RBPJ*, decreased *CD40* and subsequent decreased phosphorylation of NF-kB p65 in the ITF2357-treated FLS (Fig. 5A). To further explore the link between ITF2357 treatment and NF-kB signaling, we repeated the qPCR for the eight RA risk genes as well as *IL6* and *IL1β* regulated by NF-kB *p65* in FLS. A similar downregulation of these genes was observed in the ITF2357-treated FLS as was observed in the ITF2357-treated BL2 cells (Fig. 5B). Together, these data demonstrate the

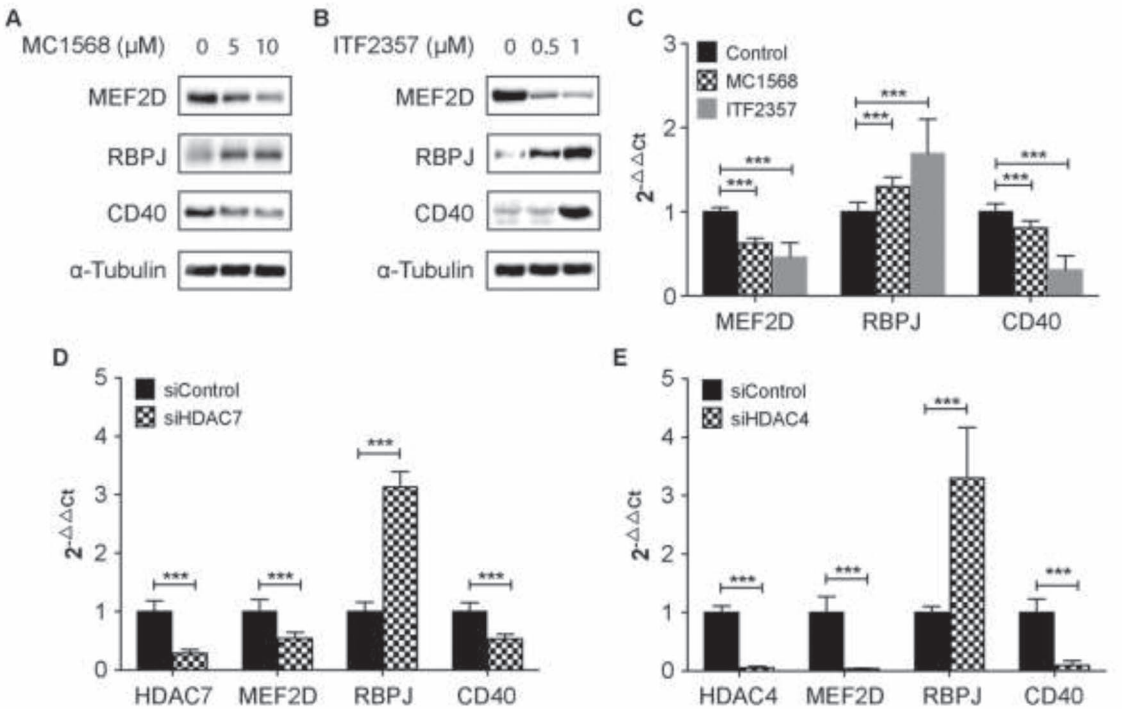

Figure 3. Effect of class II HDAC inhibitors on *MEF2D* as well as *RBPJ* and *CD40* expression in BL2 cells. (**A**, **B**) Western blots showing downregulation of *MEF2D*, upregulation of *RBPJ* and decreased expression of *CD40* in BL2 cells treated with HDAC inhibitors MC1568 and ITF2357. The data represent three biological replicates ($n = 3$). (**C**) qPCR showing downregulation of *MEF2D*, upregulation of *RBPJ* and decreased expression of *CD40* in BL2 cells treated with HDAC inhibitors MC1568 and ITF2357. The data represent a combination of three biological replicates ($n = 3$). (**D**, **E**). qPCR showing that knockdown of *HDAC7* and *HDAC4* results in downregulation of *MEF2D* and upregulation of *RBPJ*, which, in turn, decrease *CD40* expression in human primary FLS. The data represent a combination of three biological replicates ($n = 3$). ***P-value < 0.001. si, siRNA.

existence of a conserved RA-associated *CD40*-induced NF-kB STTRN in both human B cells and FLS.

ITF2357, as a prescribed drug, decreases cell migration, blocks cell cycle progression and increases apoptosis via the RA-associated *CD40*-induced NF-kB STTRN

In RA, synovial lining increases through enhanced cell migration and proliferation, and/or decreased apoptosis of fibroblast-like or macrophage-like synoviocytes, which is responsible for the synovial hyperplasia that contributes to the destruction of cartilage and bone (43). Therefore, reversal of these cellular activities has been proposed as potential options for the therapeutic intervention for RA. Among the eight risk genes that are regulated by ITF2357 in the RA-associated *CD40*-induced NF-kB STTRN, *ICAM1* is a cell adhesion molecule involved in cell migration (44). *CDK4* and *CDK6* play key roles in cell proliferation, and inhibition of *CDK4/6* expression in different RA mice models ameliorates arthritis probably by suppressing synovial hyperplasia and joint destruction (45). *c-FLIP* is a master anti-apoptotic regulator (46). To assess whether the ITF2357-treated or the *HDAC4/HDAC7* knockdown FLS reduces FLS migration, we performed a scratch-wound assay to measure basic cell migration (47). In both cases, impaired cell migration showed by delayed wound gap filling was observed (Fig. 5C and D), presumably caused by the decreased expression of *ICAM1* upon either ITF2357 treatment or the *HDAC4/HDAC7* siRNA knockdown. To determine if the ITF2357-treated or the *HDAC4/HDAC7* siRNA knockdown FLS alter cell proliferation, we performed cell cycle analysis and observed a significant G_0/G_1 phase arrest and a corresponding decrease of S and G_2/M (Fig. 5E), data that is consistent with the downregulation of *CDK4* and *CDK6* in these cells after treatment with ITF2357 or the knockdown of *HDAC4/HDAC7*. We also assessed apoptosis induced by an anti-Fas IgM monoclonal antibody (mAb) in the ITF2357-treated or the *HDAC4/HDAC7* knockdown FLS. Consistent with a previous report (48), in both ITF2357-treated or the siRNA knockdown FLS, we detected a significant increase of apoptosis that is showed by an increased caspase 3/7 activity (Fig. 5F). Together, while these data reveal the possible therapeutic effects of ITF2357 on RA, they also demonstrate the existence of the RA-associated *CD40*-induced NF-kB STTRN.

Discussion

Previously, we demonstrated that *RBPJ* suppresses *CD40* expression via binding to an RA-associated fSNP rs4810485 on the *CD40* locus in human B cells and FLS (8). Interestingly, *RBPJ* itself is also an RA risk gene. Based on GWAS catalog (2019), two LDs on the *RBPJ* locus are associated with RA. In LD with rs874040, we identified fSNPs rs17630466 and rs35944082 regulating *RBPJ* expression via binding to LEF1 and MSH6 as well as to IRF2, APOBEC3C, MEF2B and MEF2D, respectively. All these proteins were demonstrated to be the transcriptional suppressors, down-regulating *RBPJ* expression in human B cells and primary human FLS; therefore, more binding of these proteins to the risk allele G of either rs17630466 or rs35944082 will result in a decreased expression of *RBPJ*. As *RBPJ* is a transcriptional suppressor of *CD40* (8), decreased expression of *RBPJ* will lead to upregulation of *CD40*, which, in turn, can activate NF-kB p65 upon CD40L ligation. Activation of NF-kB p65 plays an important role in the pathogenesis of autoimmune diseases, such as RA, MS and

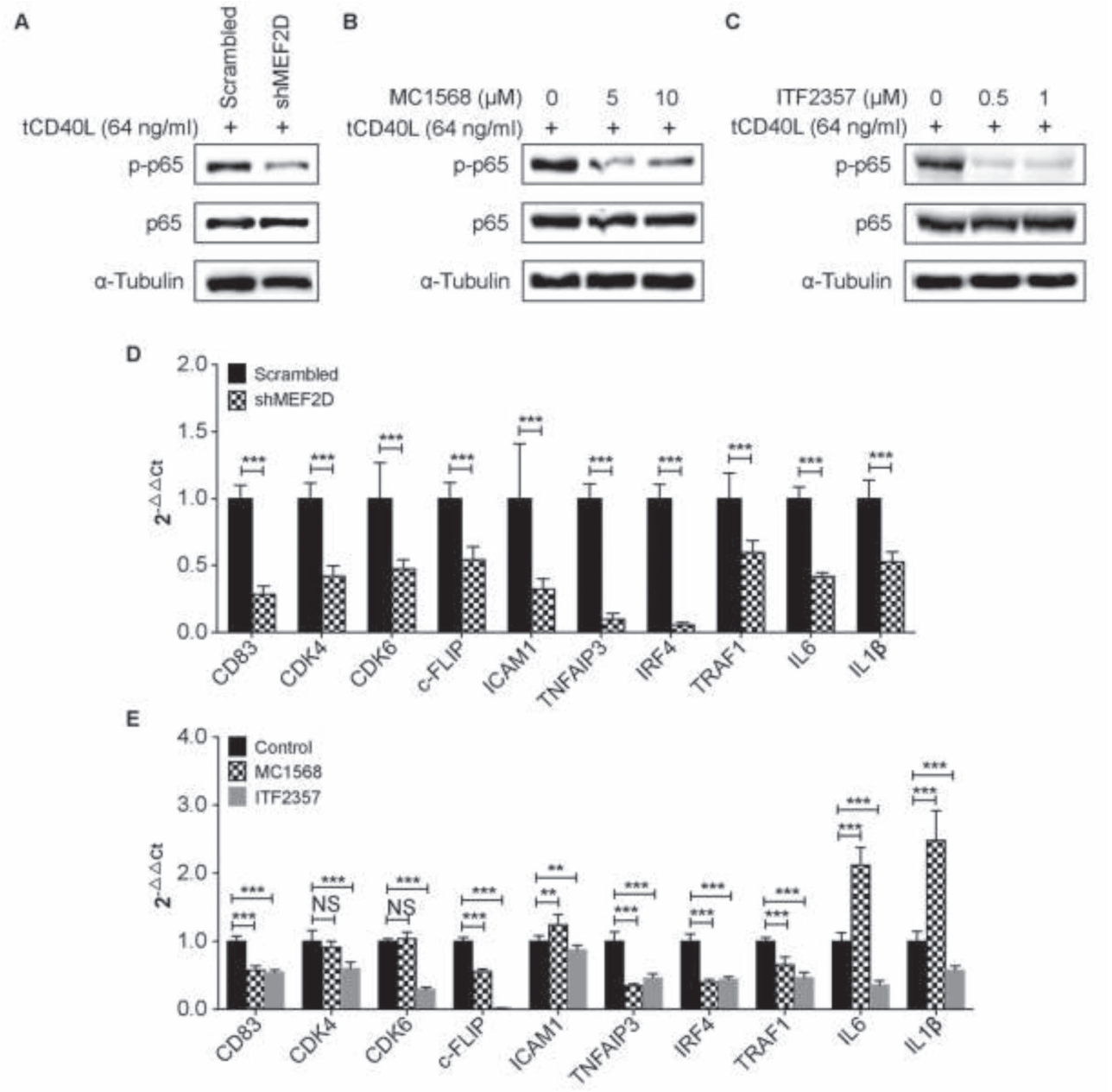

Figure 4. Inactivation of *NF-kB p65* in the *MEF2D* knockdown- and class II HDAC inhibitor-treated BL2 cells. (**A**) Western blots showing reduced phosphorylation of NF-kB p65 following *MEF2D* knockdown in BL2 cells activated by MEGACD40L. The data represent three biological replicates ($n = 3$). (**B**, **C**) Western blots showing reduced phosphorylation of NF-kB p65 in BL2 cells treated with MC1568 or ITF2357. Cells were activated with MEGACD40L following shRNA knockdown and MC1568 or ITF2357 treatment. The data represent three biological replicates ($n = 3$). p-p65: phosphorylated p65 (**D**) qPCR showing expression of the eight RA risk genes as well as *IL6* and *IL1β* in the *MEF2D* knockdown BL2 cells activated by MEGACD40L. The data represent a combination of three biological replicates ($n = 3$). (**E**) qPCR showing expression of the eight RA risk genes as well as *IL6* and *IL1β* in the BL2 cells treated with MC1568 or ITF2357. BL2 cells were activated by MEGACD40L after treatment. The data represent a combination of three biological replicates ($n = 3$). $^{**}P$-value < 0.01 and $^{***}P$-value < 0.001. sh, shRNA.

SLE (30,31). Together, these data explain the contribution of the RA-associated *RBPJ* locus to the susceptibility of RA.

Based on our findings in this work as well as in previous publications (6–8), we constructed an RA-associated *CD40*-induced NF-kB STTRN as shown in Figure 6. In this STTRN, transcriptional regulation of four RA risk genes *HADC7*, *MEF2D, RBPJ* and *CD40* is functionally linked to the transcription of other eight RA risk genes *CD83*, *CDK4/CDK6*, *c-FLIP*, *ICAM1*, *TNFAIP3*, *IRF4* and *TRAF1* as well as two proinflammatory genes *IL6* and *IL1β* via *CD40*-induced NF-kB signaling. We verified this STTRN by inactivating *HDAC4/HDAC7* either using HDAC inhibitor ITF2357 or using RNAi knockdown of *HDAC4/HDAC7*. We show that inactivation of *HDAC4/HDAC7* can result in decreased expression of *MEF2D*, which, in turn, downregulates *CD40* by suppressing *RBPJ* expression. Downregulation of *CD40* can further lead to the inactivation of NF-kB p65 by dephosphorylation, which suppresses the expression of at least 10 genes as the direct targets of NF-kB *p65*, including the eight RA risk genes as well as *IL6* and

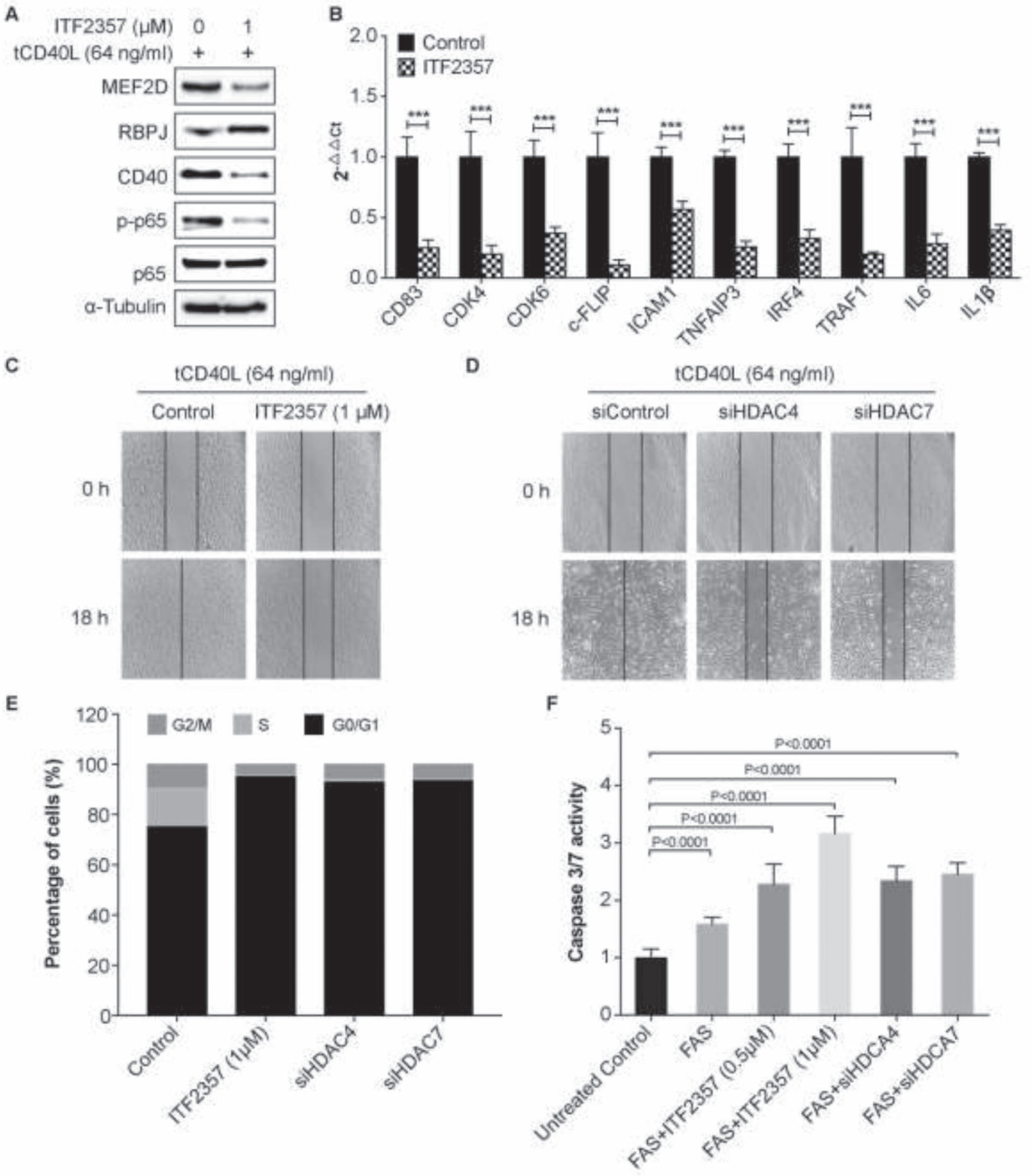

Figure 5. Demonstration of an RA-associated *CD40*-induced NF-kB STTRN in FLS. **(A)** Western blots showing that ITF2357 (1 μm) treatment in FLS cells results in inactivation of *NF-kB p65* through downregulation of *CD40*, which is caused by downregulation of *MEF2D* and upregulation of *RBPJ*. The data represent three biological replicates ($n = 3$). p-p65: phosphorylated p65 **(B)** qPCR showing downregulation of the risk genes *CDK4*, *CDK6*, *c-FLIP*, *ICAM1*, *CD83*, *TNFAIP3*, *IRF4* and *TRAF1* as well as *IL6* and *IL1β* in the ITF2357-treated FLS. FLS were activated by MEGACD40L after ITF2357 treatment. The data represent a combination of three biological replicates ($n = 3$). **(C, D)** Scratch-wound assay showing decreased cell migration in the ITF2357-treated and the *HDAC4/HDAC7* knockdown FLS. The data represent three biological replicates ($n = 3$). **(E)** Cell cycle analysis showing a G1 arrest in the ITF2357-treated and the *HDAC4/HDAC7* knockdown FLS. The data represent three biological replicates ($n = 3$). **(F)** Caspase3/7 activity analysis indicating increased apoptosis in the ITF2357-treated and the HDAC4/HDAC7 knockdown FLS. The data represent three biological replicates ($n = 3$). ***P-value < 0.001. si: siRNA.

IL1β. We also show that inactivation of *HDAC4/HDAC7*can result in decreased cell migration and proliferation and increased apoptosis, presumably via the STTRN by inactivating *ICAM1*, *CDK4/6* and *c-FLIP*. Upregulation of proinflammatory cytokines

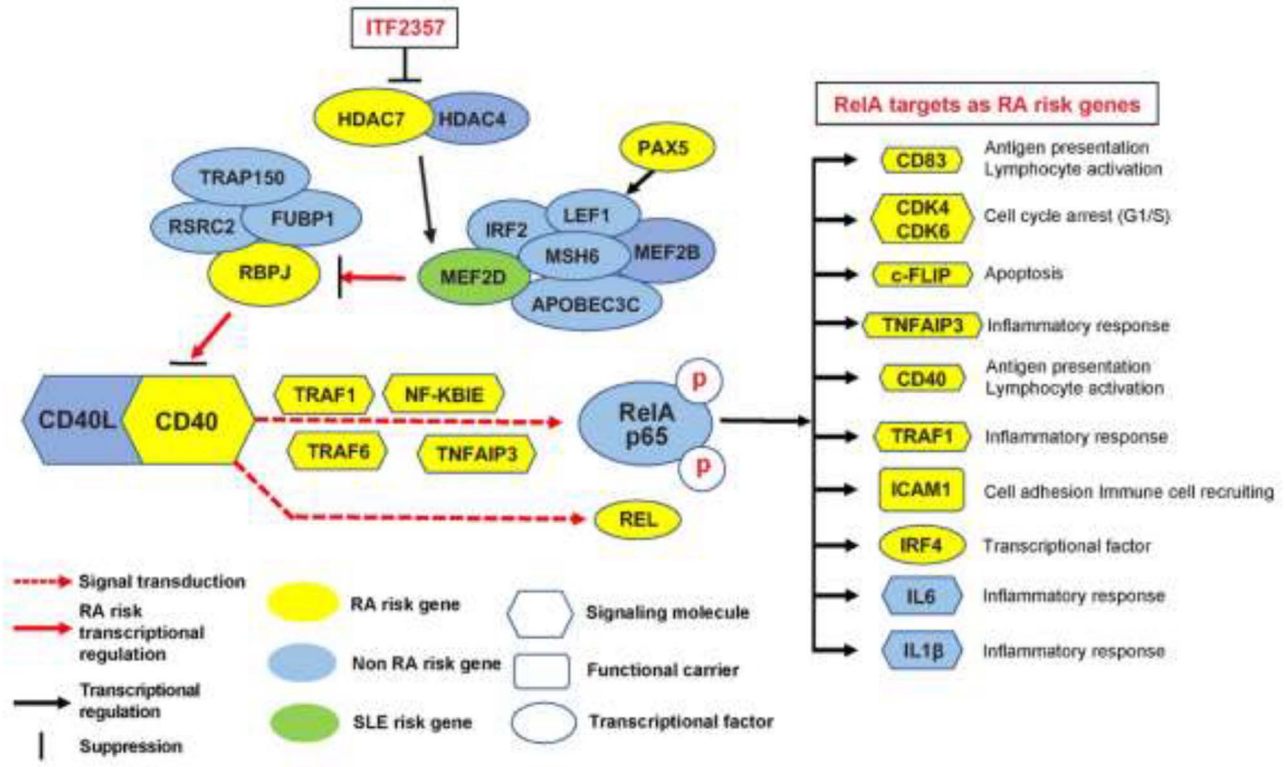

Figure 6. Scheme showing incomplete RA-associated *CD40*-induced NF-kB STTRN in human B cells and FLS. Twelve RA risk genes were shown in this RA-associated *CD40*-induced STTRN, including *HDAC7*, *MEF2D*, *RBPJ*, *CD40* as well as *CD83*, *CDK4*, *CDK6*, *c-FLIP*, *ICAM1*, *TNFAIP3*, *IRF4* and *TRAF1*. Only the transcriptional regulation of *CD40* and *RBPJ* was shown in an RA-associated fashion. *TRAF1*, *NFKBIE*, *TRAF6*, *TNFAIP3* and *REL* are the five other RA risk genes involved in *CD40*-induced NF-kB signal. RA risk gene *PAX5* could be another upstream regulator of this STTRN by modulating *LEF1* expression. ITF2357, an approved drug for SJIA, suppresses transcription of the eight RA risk genes as well as *IL6* and *IL1β* via *HDAC4/HDAC7*, *MEF2D*, *RBPJ* and *CD40* transcriptional regulation. The possible functional relevancies of these eight RA risk genes as well as *IL6* and *IL1β* are listed. *TRAF1*, *CD40* and *TNFAIP3* are in the feedback loop of transcriptional regulation via *NF-kB p65*.

IL6 and IL1β was reported in patients with RA (49,50), and increased cell migration and proliferation and decreased apoptosis in FLS were also reported to be responsible for the synovial hyperplasia that contributes to the destruction of cartilage and bone in RA (43). Therefore, inactivation of *IL6* and *IL1β*, as well as *ICAM1*, *CDK4/6* and *c-FLIP* expression, by ITF2357 reveals a novel mechanism that shows the pharmacological effect of ITF2357 as an approved drug for the treatment of SJIA. Other possible pharmacological effects of ITF2357 were reported to show that ITF2357 can also decrease disease activity by increasing the number of Treg cells and decreasing the number of TH17 cells in the arthritis mouse model (51). While both MC1568 and ITF2357 inactivate NF-kB *p65* via the RA-associated *CD40*-induced NF-kB STTRN, MC1568 alters the expression of NF-kB *p65* target genes in a different pattern, such as upregulation of *ICAM1*, *IL6* and *IL1β* expression. These differences explain why ITF2357, not MC1568, can be used as a prescribed drug for SJIA.

Many questions remain to be answered in this RA-associated *CD40*-induced NF-kB STTRN, including: (1) what are the regulatory proteins that modulate *RBPJ* expression through the other four fSNPs in LD with rs874040 on the *RBPJ* locus? Are these proteins encoded by RA risk genes or regulated by other RA risk genes? (2) How are the other RA risk genes in this STTRN regulated, especially for *HDAC7* and *MEF2D*? The association of *HDAC7* with RA and *MEF2D* with SLE has never been validated; therefore, more functional studies on these risk genes are required to determine their roles in the RA. Once all the RA-associated STTRNs are fully elucidated, the pathogenesis and susceptibility of RA could be predicted in accordance with an individual's genotype. Besides, as evidenced by our studies with ITF2357, the RA-associated STTRNs will also help develop rational strategies for the selection of therapeutic targets.

In addition, as we showed in this report, we have developed a sequential technique to perform post-GWAS functional studies by coupling SNP-seq with FREP-MS and AIDP-Wb. SNP-seq is an unbiased high-throughput screening technique to identify fSNPs based on a type IIS restriction enzyme Bpm I protection assay (8). Once we confirm the fSNPs by using EMSA and luciferase reporter assay, FREP-MS can be applied to identify proteins that specifically bind to the fSNP by enzymatically separating the fSNP sequence together with its binding proteins from the remaining DNA-nuclear extract (NE)-bead complex (8,52). After the specific binding of a regulatory protein to a fSNP is validated using AIDP-Wb (13) and ChIP assay, RNAi knockdown is performed to assess the function of the fSNP-bound proteins in regulating risk gene expression. While this approach is relatively efficient in identifying and characterizing disease-associated fSNPs, its limitation is obvious. All these techniques are *in vitro* assays using cell lines or cellular extracts, and they often do not fully represent what is occurring *in vivo*. Especially for RNAi, it is purely a loss-of-function technique that cannot identify the allele-imbalanced regulatory mechanism as a non-coding fSNP does. In consideration of these premises, we think that using CRISPR/cas9 gene editing to introduce the different alleles of a fSNP in mice would be the best approach to study non-coding fSNPs. However, this approach is currently a time-consuming

and technically difficult process; therefore, we believe that a functional validation of a fSNP *in vitro* is a guarantee for success for *in vivo* knockin studies.

In summary, we have shown an example of how to utilize post-GWAS functional studies to collect functional information for translating GWAS data into biological mechanisms. Based on these functional data, an RA-associated *CD40*-induced NF-kB STTRN was identified and validated. As *CD40*-induced NF-kB signaling is involved in many diseases, applying the same approach to identify each disease-associated, cell-type-specific *CD40*-induced NF-kB STTRN may help identify unique therapeutic targets for a range of diseases.

Materials and Methods

Cells and culture

The human B cell line BL2 was purchased from DSMZ and cultured in RPMI 1640 medium. The primary FLS were isolated from synovial tissue samples and cultured in DMEM medium. Both media were supplemented with 10% fetal bovine serum.

Fibroblast-like synoviocytes

Synovial tissue samples were collected from OA patients undergoing knee arthroplasty. The use of human materials was approved by University of Pittsburgh with the IRB number: STUDY18100138, and written informed consent was obtained from all individuals before the operative procedure. FLS were isolated from the synovial tissue samples according to a protocol previously described (53).

Primers and antibodies

All primers used in this work are listed in Supplementary Material, Table S4 and were purchased from IDT, except for *CD40*. The *CD40* primers were purchased from Genecopoeia with Cat#: HQP022955. All antibodies used are listed in Supplementary Material, Table S5 with the vendor's information.

SNP-seq

SNP-seq was performed as previously described (8). The SNP-seq library was made by the construct sequence shown in Supplementary Material, Table S4. The library was generated by Ultramer® DNA oligonucleotides (ITD) free of mutations. For fSNP screening, 100 ng of library DNA was amplified by PCR using primers bioseq and G3 for 15 cycles with AccuPrime Taq (Thermo Fisher Scientific) at 95°C for 90 s; 58°C for 90 s and 72°C for 40 s. After gel purification, 10 ng of biotinylated DNA was attached to 4 µl streptavidin-Dynabeads (Invitrogen) according to the manufacturer's protocol. The DNA-beads were then incubated with 100 µg NE for 1 h at room temperature in LightShift Chemiluminescent EMSA Kit reaction buffer (Thermo Fisher Scientific). After washing and separation, the DNA-NE-beads were digested with 2 µl Bpm I (NEB) for 30 min at 37°C. After another wash and separation, the DNA was amplified again with bioseq and G3 and re-attached to the Dynabeads for the next SNP-seq cycle. Seven cycles were performed in total with four buffer-treated controls and four NE-treated samples. Next-generation sequencing library was prepared using DNAs from cycles 1, 4 and 7 (8). Sequencing was performed using Miseq for 50 bp single end sequencing.

For quality control, we eliminated the SNPs, from which complete sequencing data were not available across cycles 1, 4 and 7, and we also eliminated the SNPs that carry mutations in the Bpm I binding sites. To identify fSNPs, we first calculated the ratio of the sequence count between the two alleles for each SNP and for each of the four replicates at cycle 7. We identified SNPs that demonstrate allele-imbalanced protection at cycle 7, with a significant difference in the ratio between the four controls and the four samples using Student's *t*-test and with a *P*-value $<$ 0.05. Second, we identified SNPs for which the allele-imbalanced protection increased with the increasing cycle number, indicating progressive enrichment. For each SNP, we calculated the average ratio of the sequence count between alleles from the four buffer-treated controls and the four NE-treated samples and normalized the ratio of the sample with the control. We next used the normalized ratio from cycles 1, 4 and 7 to calculate for Slope and identified SNPs with a Slope $>$ 0.05 and $<-$0.05 as an empirical cut-off point. We then identified candidate fSNPs with a *P*-value $<$ 0.05 and a Slope $>$ 0.05 and $<-$0.05.

Electrophoretic mobility shift assay

EMSA was performed using the LightShift Chemiluminescent EMSA Kit (Thermo Fisher) according to the manufacturer's instructions. For the probe, a 31 bp SNP fragment with the SNP centered in the middle was made by annealing two oligos. The double-stranded oligos were then biotinylated using the Biotin 3′ End DNA Labeling Kit (Thermo Fisher). The data represent three biological repeats.

FREP-MS

FREP-MS was previously described (8). In brief, ~10 µg of the purified FREP construct DNA was conjugated to 150 µl streptavidin coupled Dynabeads (Life Technologies) according to the manufacturer's instructions. The DNA-beads were then washed and mixed with 1 mg NE in a buffer from the LightShift™ Chemiluminescent EMSA Kit at RT for 1 h. After separation and washing, the DNA-NE-beads were digested with 5 µl EcoR I (100 units/µl NEB) at 37°C for 30 min to remove the 3′ DNA plus the proteins that bound to this non-SNP region. After separation and washing, the DNA-NE-beads were subsequently digested with 5 µl BamH I (100 units/µl NEB) at 37°C for 45 min to release the fSNP sequence plus the fSNP-bound proteins. The supernatant was collected for protein complex identification by mass spectrometry.

Luciferase reporter assay

Luciferase reporter assays were performed using pGL3 luciferase reporter basic vector (Cat#: E1751, Promega). Luciferase activity was measured by the Dual-Glo® Luciferase Reporter Assay System (Cat#: E2920, Promega). All the experiments were performed according to the manufacturer's protocol. Insert target sequences are listed in Supplementary Material, Table S4. All data represent a combination of six independent biological replicates.

Western blot

Whole cell proteins were isolated with RIPA buffer (Sigma). Cytosolic proteins and nuclear proteins were isolated with NE-PER Nuclear and Cytoplasmic Extraction Reagents (Thermo Scientific) according to the manufacturer's instructions. Western blots were performed using standard protocol. For control, α-tubulin was used unless as indicated. The data represent three biological replicates.

AIDP-western blot

NE was isolated as described above. A 31 bp biotinylated double-stranded DNA containing either one of the two alleles for an SNP was generated from biotinylated primers purchased from IDT by annealing. Two micrograms DNA was attached to 20 µl Dynabeads™ M-280 Streptavidin according to the manufacturer's instructions. DNA-beads were mixed with ∼100 µg NE at RT for 1 h with rotation in 50 µl binding buffer used in the LightShift Chemiluminescent kit. After magnetic separation and wash, DNA-bound proteins were eluted by adding 1× protein sample buffer and were incubated at 95°C for 5 min for western blots analysis. PARP1 was used for internal loading control. The data represent three biological replicates.

ChIP assay

ChIP was performed as described previously (54). Briefly, scrambled shRNA BL2 cells and shRNA knockdown BL2 cells were cross-linked with 1% formaldehyde for 10 min. Sonication was carried out at 30% amplitude with 20 s on and 50 s off for 5 min. Ten micrograms antibody coupled to Dynabeads™ Protein A/G (Thermo Fisher Scientific, Cat#:10001D and 10003D) was used for immunoprecipitation. DNA was purified with Qiagen PCR purification kit after reversal of the cross-link. Rabbit IgG was used as an isotype control antibody (Cell signaling Technology, Cat#: 2729). The purified DNA was used for real-time PCR analysis. The primers that were used are listed in Supplementary Material, Table S4. The data represent three biological replicates.

Real-time PCR

Total RNA was isolated with RNeasy Mini kit (Qiagen). cDNA was synthesized with SuperScript® III Reverse Transcriptase (Invitrogen) after 1 µg RNA sample was treated with DNase I (Invitrogen). All of the procedures were performed following the manufacturer's protocols. GAPDH was used as a control for all the PCR reactions. All the data represent a combination of three biological replicates unless as indicated.

RNAi knockdown

For shRNA stable knockdown in human BL2 cells, the shRNA lentiviruses were generated by cloning the targeting sequence into pLKO.1 vector (Addgene, Cat#: 10878) according to Addgene's pLKO.1 protocol. For siRNA transient knockdown in human FLS, siRNAs were purchased from Horizon Discovery, and the knockdown was performed according to the manufacturer's protocol.

MC1568 and ITF2357 treatment

BL2 cells or FLS were seeded 1 day before the treatment. On day 1, both DMSO (control) and different concentrations of MC1568 (5 and 10 µm) or ITF2357 (0.5 and 1 µm) were added. For immunoblot detection, after 24 h treatment, BL2 cells or FLS were activated either with or without MEGACD40L (64 ng/ml) for 15 min.

Scratch-wound assay

FLS were seeded into a 24 well tissue culture plate at a density of ∼60–70% confluence 1 day before the treatment. Then, cells were either treated with 1 µm ITF2357 or were transfected with siRNAs targeting both *HDAC4* and *HDAC7*. After another 24 h incubation, cells were activated by MEGACD40L at 64 ng/ml for 15 min. The monolayer cells were then gently and slowly scratched with a 200 µl pipette tip across the center of the well. After scratching, the detached cells were gently removed by washing and the well was replenished with fresh medium. After another 18 h incubation, photos were taken. The data represent three biological replicates.

Cell proliferation analysis

1X10 (5) FLS were seeded in a six well plate 1 day before the treatment. Cells were then either treated with 0.5 and 1 µm ITF2357 or were transfected with siRNAs targeting both *HDAC4* and *HDAC7* for 24 h. Cells were then further activated by MEGACD40L at 64 ng/ml for 15 min and were stained with 20 µl of 500 µg/ml propidium iodide (Biolegeng, Cat#: 421301) according to the manufacturer's protocol. Data were collected by Attune™ NxT Flow Cytometer Software (Thermo Fisher Scientific) and FlowJo version 6. The data represent three biological replicates.

Caspase-Glo® 3/7 assay

1X10 (4) FLS were seeded in a 96 well plate 1 day before the treatment. Then, cells were either treated with 0.5 and 1 µm ITF2357 or were transfected with siRNAs targeting both HDAC4 and HDAC7. After 24 h incubation, cells were further activated by MEGACD40L at 64 ng/ml for 15 min and were induced for apoptosis by exposing the cells to anti-Fas IgM mAb (MyBioSource Cat#: MBS485033MBL) at 1 µg/ml for another 24 h as previously described (48). Apoptosis was evaluated by detecting the caspase 3/7 activities using Caspase-Glo® 3/7 assay system (Cat#: G8091, Promega) according to the manufacturer's protocol. Fluorescence was read at 485 nm excitation, 520 nm emission, followed by luminescence. The data represent a combination of three biological replicates.

Statistical analysis

P-values were calculated using Student's *t*-test with two tails. Error bars represent the median with standard error (S.E.)

Supplementary Material

Supplementary Material is available at *HMG* online.

Acknowledgements

We thank Drs Toren Finkel and Jie Liu for scientific discussions concerning this work. This work was supported by grants from the Arthritis National Research Foundation (to G.L.), National Multiple Sclerosis Society (to G.L.) and National Institute of Health (R21 NS096443 and R21 AR070378 to G.L.).

Conflict of Interest statement. None declared.

References

1. Scott, D.L., Wolfe, F. and Huizinga, T.W. (2010) Rheumatoid arthritis. *Lancet*, **376**, 1094–1108.
2. Okada, Y., Diogo, D., Greenberg, J.D., Mouassess, F., Achkar, W.A., Fulton, R.S., Denny, J.C., Gupta, N., Mirel, D., Gabriel,

S. et al. (2014) Integration of sequence data from a consanguineous family with genetic data from an outbred population identifies PLB1 as a candidate rheumatoid arthritis risk gene. *PLoS One*, **9**, e87645.
3. (2014) Little boxes. *Nat. Genet.*, **46**, 659.
4. Deane, K.D., Striebich, C.C. and Holers, V.M. (2017) Editorial: prevention of rheumatoid arthritis: now is the time, but how to proceed? *Arthritis Rheumatol.*, **69**, 873–877.
5. Schonbeck, U. and Libby, P. (2001) The *CD40*/CD154 receptor/ligand dyad. *Cell. Mol. Life Sci.*, **58**, 4–43.
6. Okada, Y., Wu, D., Trynka, G., Raj, T., Terao, C., Ikari, K., Kochi, Y., Ohmura, K., Suzuki, A., Yoshida, S. *et al.* (2014) Genetics of rheumatoid arthritis contributes to biology and drug discovery. *Nature*, **506**, 376–381.
7. Li, G., Diogo, D., Wu, D., Spoonamore, J., Dancik, V., Franke, L., Kurreeman, F., Rossin, E.J., Duclos, G., Hartland, C. *et al.* (2013) Human genetics in rheumatoid arthritis guides a high-throughput drug screen of the *CD40* signaling pathway. *PLoS Genet.*, **9**, e1003487.
8. Li, G., Martinez-Bonet, M., Wu, D., Yang, Y., Cui, J., Nguyen, H.N., Cunin, P., Levescot, A., Bai, M., Westra, H.J. *et al.* (2018) High-throughput identification of noncoding functional SNPs via type IIS enzyme restriction. *Nat. Genet.*, **50**, 1180–1188.
9. Stahl, E.A., Raychaudhuri, S., Remmers, E.F., Xie, G., Eyre, S., Thomson, B.P., Li, Y., Kurreeman, F.A., Zhernakova, A., Hinks, A. *et al.* (2010) Genome-wide association study meta-analysis identifies seven new rheumatoid arthritis risk loci. *Nat. Genet.*, **42**, 508–514.
10. Chatzigeorgiou, A., Lyberi, M., Chatzilymperis, G., Nezos, A. and Kamper, E. (2009) *CD40*/CD40L signaling and its implication in health and disease. *Biofactors*, **35**, 474–483.
11. Zhang, B., Wu, T., Chen, M., Zhou, Y., Yi, D. and Guo, R. (2013) The *CD40*/CD40L system: a new therapeutic target for disease. *Immunol. Lett.*, **153**, 58–61.
12. Chen, L. and Wu, J. (2012) Systems biology for complex diseases. *J. Mol. Cell Biol.*, **4**, 125–126.
13. Zhao, Y., Wu, D., Jiang, D., Zhang, X., Wu, T., Cui, J., Qian, M., Zhao, J., Oesterreich, S., Sun, W. *et al.* (2020) A sequential methodology for the rapid identification and characterization of breast cancer-associated functional SNPs. *Nat. Commun.*, **11**, 1–10.
14. Ward, L.D. and Kellis, M. (2012) HaploReg: a resource for exploring chromatin states, conservation, and regulatory motif alterations within sets of genetically linked variants. *Nucleic Acids Res.*, **40**, D930–D934.
15. Sur, I., Tuupanen, S., Whitington, T., Aaltonen, L.A. and Taipale, J. (2013) Lessons from functional analysis of genome-wide association studies. *Cancer Res.*, **73**, 4180–4184.
16. Visel, A., Rubin, E.M. and Pennacchio, L.A. (2009) Genomic views of distant-acting enhancers. *Nature*, **461**, 199–205.
17. Maurano, M.T., Humbert, R., Rynes, E., Thurman, R.E., Haugen, E., Wang, H., Reynolds, A.P., Sandstrom, R., Qu, H., Brody, J. *et al.* (2012) Systematic localization of common disease-associated variation in regulatory DNA. *Science*, **337**, 1190–1195.
18. Gaffney, D.J. (2013) Global properties and functional complexity of human gene regulatory variation. *PLoS Genet.*, **9**, e1003501.
19. Battle, A. and Montgomery, S.B. (2014) Determining causality and consequence of expression quantitative trait loci. *Hum. Genet.*, **133**, 727–735.
20. Dickel, D.E., Visel, A. and Pennacchio, L.A. (2013) Functional anatomy of distant-acting mammalian enhancers. *Philos. Trans. R. Soc. Lond. B Biol. Sci.*, **368**, 20120359.
21. Jenkins, M.A. (2009) Role of MSH6 and PMS2 in the dna mismatch repair process and carcinogenesis. *Surg. Oncol. Clin. N. Am.*, **18**, 625–636.
22. Jolma, A., Yan, J., Whitington, T., Toivonen, J., Nitta, K.R., Rastas, P., Morgunova, E., Enge, M., Taipale, M., Wei, G. *et al.* (2013) DNA-binding specificities of human transcription factors. *Cell*, **152**, 327–339.
23. Palma-Vera, S.E. and Einspanier, R. (2016) Experimental and bioinformatic analysis of cultured bovine endometrial cells (BEND) responding to interferon tau (IFNT). *Reprod. Biol. Endocrinol.*, **14**, 22.
24. Farias, F.H.G., Dahlqvist, J., Kozyrev, S.V., Leonard, D., Wilbe, M., Abramov, S.N., Alexsson, A., Pielberg, G.R., Hansson-Hamlin, H., Andersson, G. *et al.* (2019) A rare regulatory variant in the MEF2D gene affects gene regulation and splicing and is associated with a SLE sub-phenotype in Swedish cohorts. *Eur. J. Hum. Genet.*, **27**, 432–441.
25. Toro-Dominguez, D., Carmona-Saez, P. and Alarcon-Riquelme, M.E. (2014) Shared signatures between rheumatoid arthritis, systemic lupus erythematosus and Sjogren's syndrome uncovered through gene expression meta-analysis. *Arthritis Res. Ther.*, **16**, 489.
26. Nebbioso, A., Manzo, F., Miceli, M., Conte, M., Manente, L., Baldi, A., De Luca, A., Rotili, D., Valente, S., Mai, A. *et al.* (2009) Selective class II HDAC inhibitors impair myogenesis by modulating the stability and activity of HDAC-MEF2 complexes. *EMBO Rep.*, **10**, 776–782.
27. Vojinovic, J. and Damjanov, N. (2011) HDAC inhibition in rheumatoid arthritis and juvenile idiopathic arthritis. *Mol. Med.*, **17**, 397–403.
28. Daneshpajooh, M., Eliasson, L., Bacos, K. and Ling, C. (2018) MC1568 improves insulin secretion in islets from type 2 diabetes patients and rescues beta-cell dysfunction caused by Hdac7 upregulation. *Acta Diabetol.*, **55**, 1231–1235.
29. Ellinghaus, D., Jostins, L., Spain, S.L., Cortes, A., Bethune, J., Han, B., Park, Y.R., Raychaudhuri, S., Pouget, J.G., Hubenthal, M. *et al.* (2016) Analysis of five chronic inflammatory diseases identifies 27 new associations and highlights disease-specific patterns at shared loci. *Nat. Genet.*, **48**, 510–518.
30. Scheinman, R. (2013) NF-kappaB and rheumatoid arthritis: will understanding genetic risk lead to a therapeutic reward? *For Immunopathol. Dis. Therap.*, **4**, 93–110.
31. Noort, A.R., Tak, P.P. and Tas, S.W. (2015) Non-canonical NF-kappaB signaling in rheumatoid arthritis: Dr Jekyll and Mr Hyde? *Arthritis Res. Ther.*, **17**, 15.
32. Criswell, L.A. (2010) Gene discovery in rheumatoid arthritis highlights the *CD40*/NF-kappaB signaling pathway in disease pathogenesis. *Immunol. Rev.*, **233**, 55–61.
33. Liu, T., Zhang, L., Joo, D. and Sun, S.C. (2017) NF-kappaB signaling in inflammation. *Signal Transduct. Target. Ther.*, **2**, 17023.
34. Han, H., Cho, J.W., Lee, S., Yun, A., Kim, H., Bae, D., Yang, S., Kim, C.Y., Lee, M., Kim, E. *et al.* (2018) TRRUST v2: an expanded reference database of human and mouse transcriptional regulatory interactions. *Nucleic Acids Res.*, **46**, D380–D386.
35. Kretschmer, B., Kuhl, S., Fleischer, B. and Breloer, M. (2011) Activated T cells induce rapid *CD83* expression on B cells by engagement of *CD40*. *Immunol. Lett.*, **136**, 221–227.
36. Ishida, T., Kobayashi, N., Tojo, T., Ishida, S., Yamamoto, T. and Inoue, J. (1995) *CD40* signaling-mediated induction of Bcl-XL,

Cdk4, and *Cdk6*. Implication of their cooperation in selective B cell growth. *J. Immunol.*, **155**, 5527–5535.
37. Travert, M., Ame-Thomas, P., Pangault, C., Morizot, A., Micheau, O., Semana, G., Lamy, T., Fest, T., Tarte, K. and Guillaudeux, T. (2008) *CD40* ligand protects from TRAIL-induced apoptosis in follicular lymphomas through NF-kappaB activation and up-regulation of *c-FLIP* and Bcl-xL. *J. Immunol.*, **181**, 1001–1011.
38. Yellin, M.J., Winikoff, S., Fortune, S.M., Baum, D., Crow, M.K., Lederman, S. and Chess, L. (1995) Ligation of *CD40* on fibroblasts induces CD54 (ICAM-1) and CD106 (VCAM-1) up-regulation and IL-6 production and proliferation. *J. Leukoc. Biol.*, **58**, 209–216.
39. Sarma, V., Lin, Z., Clark, L., Rust, B.M., Tewari, M., Noelle, R.J. and Dixit, V.M. (1995) Activation of the B-cell surface receptor *CD40* induces A20, a novel zinc finger protein that inhibits apoptosis. *J. Biol. Chem.*, **270**, 12343–12346.
40. Saito, M., Gao, J., Basso, K., Kitagawa, Y., Smith, P.M., Bhagat, G., Pernis, A., Pasqualucci, L. and Dalla-Favera, R. (2007) A signaling pathway mediating downregulation of BCL6 in germinal center B cells is blocked by BCL6 gene alterations in B cell lymphoma. *Cancer Cell*, **12**, 280–292.
41. Georgopoulos, N.T., Steele, L.P., Thomson, M.J., Selby, P.J., Southgate, J. and Trejdosiewicz, L.K. (2006) A novel mechanism of *CD40*-induced apoptosis of carcinoma cells involving TRAF3 and JNK/AP-1 activation. *Cell Death Differ.*, **13**, 1789–1801.
42. Ospelt, C. (2017) Synovial fibroblasts in 2017. *RMD Open*, **3**, e000471.
43. Perlman, H., Pagliari, L.J. and Volin, M.V. (2001) Regulation of apoptosis and cell cycle activity in rheumatoid arthritis. *Curr. Mol. Med.*, **1**, 597–608.
44. Lyck, R. and Enzmann, G. (2015) The physiological roles of ICAM-1 and ICAM-2 in neutrophil migration into tissues. *Curr. Opin. Hematol.*, **22**, 53–59.
45. Sekine, C., Sugihara, T., Miyake, S., Hirai, H., Yoshida, M., Miyasaka, N. and Kohsaka, H. (2008) Successful treatment of animal models of rheumatoid arthritis with small-molecule cyclin-dependent kinase inhibitors. *J. Immunol.*, **180**, 1954–1961.
46. Safa, A.R. (2012) *c-FLIP*, a master anti-apoptotic regulator. *Exp. Oncol.*, **34**, 176–184.
47. Martinotti, S. and Ranzato, E. (2019) Scratch wound healing assay. *Methods Mol. Biol.*
48. Palao, G., Santiago, B., Galindo, M., Paya, M., Ramirez, J.C. and Pablos, J.L. (2004) Down-regulation of FLIP sensitizes rheumatoid synovial fibroblasts to Fas-mediated apoptosis. *Arthritis Rheum.*, **50**, 2803–2810.
49. Hashizume, M. and Mihara, M. (2011) The roles of interleukin-6 in the pathogenesis of rheumatoid arthritis. *Arthritis*, **2011**, 765624.
50. Choy, E.H. and Panayi, G.S. (2001) Cytokine pathways and joint inflammation in rheumatoid arthritis. *N. Engl. J. Med.*, **344**, 907–916.
51. Nijhuis, L., Peeters, J.G.C., Vastert, S.J. and van Loosdregt, J. (2019) Restoring T cell tolerance, exploring the potential of histone deacetylase inhibitors for the treatment of juvenile idiopathic arthritis. *Front. Immunol.*, **10**, 151.
52. Li, G., Cunin, P., Wu, D., Diogo, D., Yang, Y., Okada, Y., Plenge, R.M. and Nigrovic, P.A. (2016) The rheumatoid arthritis risk variant CCR6DNP regulates CCR6 via PARP-1. *PLoS Genet.*, **12**, e1006292.
53. Kiener, H.P., Lee, D.M., Agarwal, S.K. and Brenner, M.B. (2006) Cadherin-11 induces rheumatoid arthritis fibroblast-like synoviocytes to form lining layers *in vitro*. *Am. J. Pathol.*, **168**, 1486–1499.
54. Noss, E.H., Nguyen, H.N., Chang, S.K., Watts, G.F. and Brenner, M.B. (2015) Genetic polymorphism directs IL-6 expression in fibroblasts but not selected other cell types. *Proc. Natl. Acad. Sci. U. S. A.*, **112**, 14948–14953.